

# Deformation and toughness of polymeric systems: 5. A critical examination of multilayered structures

M. C. M. van der Sanden\*, L. G. C. Buijs, F. O. de Bie and H. E. H. Meijer†

Centre for Polymers and Composites (CPC), Eindhoven University of Technology,

PO Box 513, 5600 MB Eindhoven, The Netherlands

(Received 2 June 1993; revised 3 December 1993)

The deformation behaviour of multilayered tapes based on polystyrene–poly(2,6-dimethyl-1,4-phenylene ether) (PS-PPE) and polyethylene (PE) layers is investigated for PS-PPE layer thicknesses varying from 50 down to 0.05  $\mu\text{m}$ . Two (rather than one) transitions can be observed in decreasing the PS-PPE layer thickness ( $d$ ). The first transition at  $d \approx 1 \mu\text{m}$  is enabled by a stress transfer mechanism that is similar to the mechanism operating in fragmentation tests in fibre reinforced composites and is operative through the non-zero but still low level of interlayer adhesion ( $G_{ic} \approx 5 \text{ J m}^{-2}$ ) between PS-PPE and PE. This can be exploited practically by the introduction of a significant level of interlayer adhesion via the incorporation of a diblock copolymer between the PS-PPE and PE layers which, finally, results in a multilayered system with a strain-to-break of pure PE. The second transition at  $0.5 \mu\text{m} > d > 0.05 \mu\text{m}$  (dependent on the network density) is associated with a change in deformation mechanism from crazing to shear deformation as revealed by optical light microscopy during tensile testing. The strain-to-break below the second transition corresponds to a value comparable with the stretching of the entanglement network to its full extension ( $\lambda_{\text{max}}$ ). The critical layer thickness found coincides with the experimentally determined critical thickness as already reported for the non-adhering core–shell rubber-modified PS-PPE systems in part 2 of this series. The absolute value of the critical layer/ligament thickness and its dependence on the network density can be explained by the previously introduced energy-based model or, alternatively, by the detailed micromechanical analysis of the craze growth mechanism as proposed by Kramer.

(Keywords: deformation; multilayered tapes; network density)

## INTRODUCTION

In parts 1 and 2 of this series<sup>1,2</sup> the concept of a material-specific thickness, below which brittle, amorphous glassy polymers become ductile, was introduced. It was shown that the value of the critical thickness as well as the maximum level of ductility are both determined by the molecular (network) structure of the polymer. Using thin sheets in stratified structures (with a non-adhering polymer as a spacer) the onset to the sudden increase in macroscopic strain-to-break was demonstrated while for thin ligaments in between 'holes' (i.e. non-adhering core–shell rubbery particles) it was shown that the macroscopic strain-to-break of brittle, amorphous polymers can be increased to 60% of the theoretical strain-to-break based on the stretching of a single entanglement strand of the network structure to its full extension.

Since in part 2 attention was focused on the understanding of the phenomenon of the material-specific critical thickness, mainly the core–shell rubber-modified structures were discussed. Here, the deformation behaviour of multilayered tapes based on polystyrene–poly(2,6-dimethyl-1,4-phenylene ether) (PS-PPE) layers

alternating with polyethylene (PE) is studied in more detail. PE is used as a non-adhering spacer possessing a constant high level of ductility at all layer thicknesses<sup>1</sup>. The number of layers in the tape (and thus the PS-PPE layer thickness,  $d$ ) can be set by changing the number of mixing elements in the Multiflux static mixer used<sup>1</sup> while keeping the total tape thickness constant. However, the viscosity ratio of both components proves to determine the maximum number of elements and thus the limiting layer thicknesses since, finally, viscosity and normal stress difference driven interfacial instabilities render layer break-up and rupture<sup>3–5</sup>. As an example of the opposite, for the system polystyrene/poly(methyl methacrylate) (PS/PMMA) 50/50, with fairly matching flow curves within the shear rate and temperature range applied, a spectacular minimum layer thickness of 40 nm could be achieved (Figure 1). In the PS-PPE/PE systems no attempt was made to properly optimize the viscosity ratio (e.g. by choosing different PE types for the different PS-PPE compositions) since attention is focused on the micromechanical explanation of the deformation behaviour found for the different network structures and test geometries.

The motivation for this more detailed investigation on especially the multilayered tapes originated from some stimulating criticism met in the early stage of our research: when we first presented the striking experimental findings

\* Present address: Physics Department, University of California at Santa Barbara, Broida Hall, Santa Barbara, CA 93106, USA

† To whom correspondence should be addressed

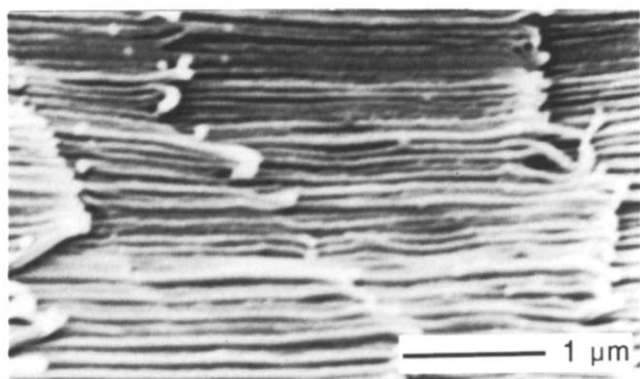


**Figure 1** SEM micrograph of a multilayered PS/PMMA 50/50 tape (layer thickness: 40 nm)

concerning the material-dependent critical thickness (read: thinness) in January 1992 to some experts in the area of micromechanics of polymers, both Kramer (Cornell University) and Baer (Case Western Reserve University) noticed the possible importance of a small level of adhesion that is always present in thin multilayered structures even if immiscible polymer pairs (like PS and PE) are used. This especially could be of influence in the interpretation of the results on the stratified structures. The convincing results of the extremely different macroscopic deformation behaviour of 60 wt% adhering (PS-shell) and non-adhering (PMMA shell) core-shell rubber-modified PS<sup>1</sup> made the interpretation of the experimental findings in these systems less ambiguous and, finally, resulted in the simple energy-based model that is capable of describing the criterion for macroscopic ductility in crazing and shear deforming polymers (including thermosets!)<sup>2,6,7</sup>. The application of this model to predict the change in strain-to-break of the continuous thin stratified multilayered structures is, however, not that straightforward and needs some additional assumptions. Both aspects are dealt with in this paper: using the micromechanical facilities in Case Western Reserve University, the details of the deformation behaviour of our tapes were revealed, while Kramer reworked, after a number of subsequent discussions also at our laboratory, his existing model (that is focused especially on the transition from crazing to shearing)<sup>8</sup> to include the network density effect as found in our previous experiments and is easily applicable to thin films as well.

Several studies have been reported on microlayered structures focusing on unique properties with respect to their optical, barrier and mechanical properties<sup>9-11</sup>. The strain-to-break of multilayered systems containing at least one ductile component can be improved via three routes: (i) a decrease of the layer thickness of the brittle component; this finally results in an elimination of the limiting effect to the overall strain-to-break<sup>1,2</sup> while, (ii) the introduction of a considerable degree of adhesion between the layers of the brittle and ductile component can result in a mutual induction of deformation mechanisms in both types of layers<sup>12,13</sup> and, (iii) also can allow for multiple fracture of each separate brittle layer<sup>14</sup>.

In this study the adhesion ( $G_{IC}$ ) between the PS-PPE and PE layers is investigated by applying a double cantilever beam (DCB) peel test as described by Bazhenov *et al.*<sup>15</sup> and optical light microscopy during uniaxial

tensile testing is applied to elucidate the deformation mechanism of the PS-PPE/PE tapes. In order to gain some more insight into the phenomenon of interlayer adhesion, a third component (a diblock copolymer) between every individual PS-PPE and PE layer has been introduced to influence the adhesion in a rather extreme and precise manner.

## EXPERIMENTAL

### Materials

The materials used were PS (Dow Styron 638), PPE (General Electric Co., PPE-803), low-density PE (DSM, LDPE 1808 AN) and a diblock copolymer based on PS and hydrogenated isoprene rubber (Shell, Kraton G-1701 X). PS and PPE were mixed in various proportions (100-0, 80-20, 60-40 and 40-60) to set the entanglement density of the PS-PPE blend (see ref. 2 for a detailed description of the mixing procedure). The diblock copolymer used ( $M_n = 82 \text{ kg mol}^{-1}$ ,  $M_w = 88 \text{ kg mol}^{-1}$ ) contains ~37 wt% PS.

### Sample preparation

PS-PPE and PE were multilayered in different compositions (100/0, 75/25, 50/50, 25/75 and 0/100) using the Multiflux mixer that renders the most perfect baker's transformation of all mixers<sup>16</sup>. Laminated tapes with different spacing PE layers were prepared at 200°C (PS-PPE: 100-0), 220°C (PS-PPE: 80-20), 225°C (PS-PPE: 60-40) and 230°C (PS-PPE: 40-60). The total number of continuous layers that could be obtained in a tape varied between 128 (6 mixing elements) and 4096 (11 mixing elements; see comments on the influence of the viscosity ratio in the Introduction) while the total tape thickness was kept constant around 0.3 mm. Multilayered tapes will be indicated with a three number code: A-B/C, where A-B is the PS-PPE composition of the tape and C is the weight fraction of PE in the tape.

Multilayered tapes containing the diblock copolymer (BC) as a third component were prepared at 200°C for the pure PS/PE system only. Four ingoing layers are required in this case, stacked as: PS/BC/PE/BC. Three different PS/PE ratios were chosen (75/25, 50/50 and 25/75) while the total amount of block copolymer was 1 wt%.

Small dumb-bell shaped tensile specimens were machined from the multilayered tapes parallel to the direction of extrusion according to ASTM D 1708.

To avoid any unwanted orientation effects, prior to mechanical analysis all machined tapes were annealed for 24 h at a temperature 20°C below the glass transition temperature ( $T_g$ ) of the PS-PPE phase. Heating of the samples at a temperature of 10°C above the  $T_g$  of the PS-PPE phase revealed a shrinkage of ~4%. This value should not have a noticeable influence on the mechanical properties of the tapes<sup>17,18</sup>.

### Interlayer adhesion

The interlayer adhesion of several tapes was measured using a (modified) DCB peel test as described by Bazhenov *et al.*<sup>15</sup>. The conventional DCB test could not be used because this test does not allow for a substantial bending of the beams, which occurred in our situation. Adhesion in the modified DCB test<sup>15</sup> is characterized by the fracture toughness ( $G_{IC}$ ), i.e. the energy dissipated

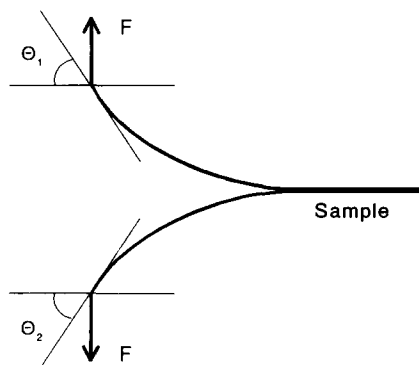


**Figure 2** Schematic representation of the modified double cantilever beam peel test

during the formation of new surface, given by:

$$G_{Ic} = \frac{F(\sin \Theta_1 + \sin \Theta_2)}{W} \quad (1)$$

where  $F$  is the peel force,  $\Theta_1$  and  $\Theta_2$  are the angles between the cantilever beam ends and the direction of the force applied (*Figure 2*) and  $W$  is the width of the sample (5 mm). Specimens were cut from the extruded tapes with a diamond saw into the desired dimensions (length  $\times$  width: 90 mm  $\times$  10 mm). An initial crack (depth: 10 mm) was made as close as possible to the middle level of the sample using a fresh razor blade. Subsequently, tabs were glued on the end of both cantilever beams and force was applied (*Figure 2*) using an Instron tensile testing machine equipped with a 5 N load cell at a loading rate of 10 mm min<sup>-1</sup>. The cantilever beam end angles during crack propagation were determined by taking photographs periodically. Three samples (of the same composition) were tested in order to obtain an average value of  $G_{Ic}$ .

#### Microscopy

Optical reflecting light microscopy (Olympus BH equipped with a C-35AD-2 Olympus camera) was applied to investigate the fracture surface after measuring the interlayer adhesion in order to verify the crack propagation path.

Scanning electron microscopy (SEM) was applied to check the thickness and homogeneity of the PS-PPE layers. Specimens were cut from the centre of the layered specimen, parallel to the direction of extrusion and perpendicular to the layers. The surface was microtomed using a glass knife at liquid-nitrogen temperature, subsequently etched in an oxygen plasma to remove the PE (and rubber-phase of the diblock copolymer) and finally covered with a conducting gold layer.

#### Mechanical testing

Multilayered tapes were uniaxially strained on a Frank tensile machine (type: 81565 IV) at a cross-head speed of 5 mm min<sup>-1</sup> ( $l_0 = 20$  mm). In order to obtain representative data, all experiments were carried out five times for each testing condition. Strain was directly derived from cross-head displacements.

#### Microscopy during tensile testing

To visualize the deformation behaviour, deformation was realized using a Minimat (Polymer Laboratories;

distance between clamps: 15 mm) mounted on an optical transmission microscope (Olympus BH2). Dumb-bell shaped tensile specimens were viewed in transmission perpendicular to the tape surface at a low testing speed (5 mm min<sup>-1</sup>) at Case Western Reserve University (Cleveland). Before testing the top and bottom layers were peeled off (easily achieved in the poorly adhering PS-PPE/PE systems) to remove any irregularities and to ensure that all tapes had the same thickness (0.3 mm). During loading pictures were taken at distinct stages of the deformation using an Olympus C-35 AD-2 camera mounted on the microscope. Plastic (shear) deformation, if present, could be visualized with a polarizing filter added to improve the colour contrast.

## RESULTS AND DISCUSSION

### Interfacial adhesion

*Figure 3* demonstrates the interlayer adhesion as determined using the (modified) DCB test of several PS-PPE/PE tapes: 100-0/75, 60-40/75 and 60-40/50 versus the PS-PPE layer thickness. From *Figure 3* it can be inferred that the  $G_{Ic}$  value for all PS-PPE layer thicknesses is very low (5–25 J m<sup>-2</sup>) compared with the values published for the PC/SAN system: 100–1200 J m<sup>-2</sup> (refs 15 and 19) and independent of the ratio PS-PPE/PE. The amount of PPE present in the PS-PPE phase does not influence the interlayer adhesion but, surprisingly, the PS-PPE layer thickness has a pronounced influence on the  $G_{Ic}$  value: with a decreasing PS-PPE layer thickness the interlayer adhesion increases significantly. Examination of the fracture surfaces of the delaminated samples elucidates the increasing  $G_{Ic}$  values with a decreasing PS-PPE layer thickness (*Figure 4*; crack path direction: vertical). In *Figure 4a* (100-0/75; PS-PPE layer thickness: 1  $\mu$ m) a clear fracture surface can be observed. Decreasing the PS-PPE layer thickness results in a fracture surface that is covered with torn layers (*Figure 4b*) or even demonstrates a large amount of plastic deformation (*Figure 4c*). Hence, the increased  $G_{Ic}$  interlayer adhesion values are caused by a multiple crack propagation path. Consequently, the  $G_{Ic}$

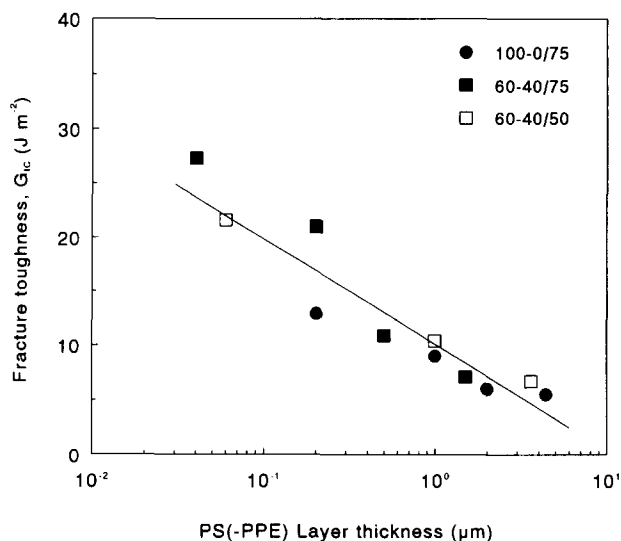


**Figure 3** Interlayer adhesion ( $G_{Ic}$ ) of 100-0/75, 60-40/75 and 60-40/50 tapes versus the PS-PPE layer thickness

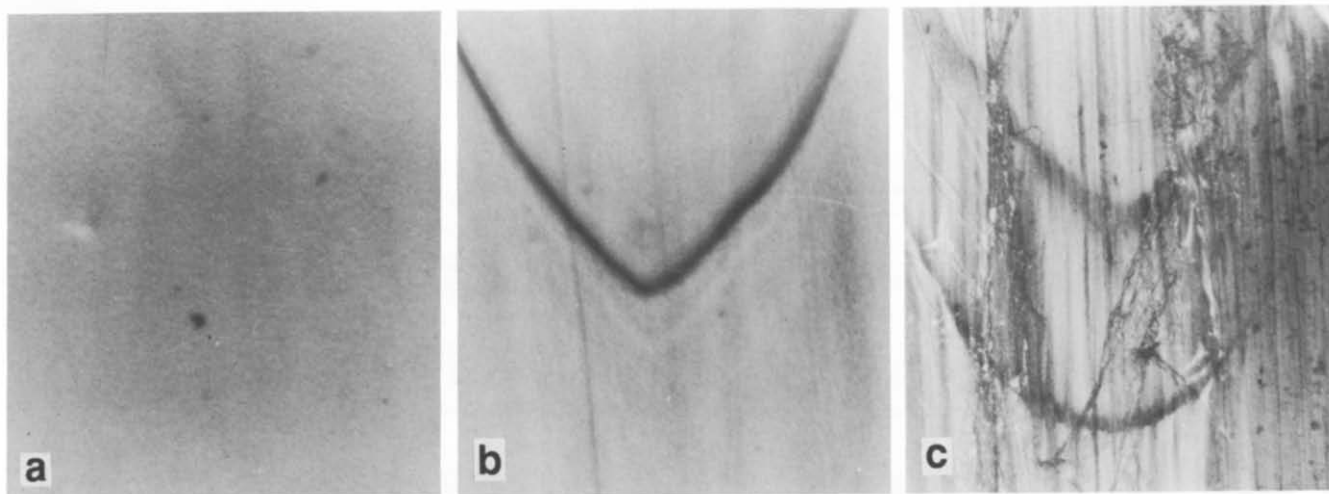


**Figure 4** Optical micrographs of the crack path of PS-PPE multilayered tapes after measuring the interlayer adhesion ( $G_{1c}$ ): (a) 100-0/75, PS-PPE layer thickness: 1  $\mu\text{m}$ ; (b) 60-40/75, PS-PPE layer thickness: 0.5  $\mu\text{m}$ ; and (c) 60-40/75, PS-PPE layer thickness: 0.04  $\mu\text{m}$

interlayer adhesion obtained from a 100-0/75 tape with a PS-PPE layer thickness of  $\sim 1 \mu\text{m}$  (corresponding to the delaminated fracture surface of *Figure 4a*) is the most representative value ( $5 \text{ J m}^{-2}$ ), which is a very low value as already stated above.

#### Mechanical testing

*Figure 5* shows the strain-to-break of several multilayered PS-PPE/PE tapes (100-0/ $X$ , 80-20/ $X$ , 60-40/ $X$  and 40-60/ $X$ ) versus the PS-PPE layer thickness. The strain-to-break of the tape is defined as the strain at which a sharp decrease in stress is observed (see *Figure 4* in ref. 1) corresponding to the breakage of the PS-PPE layers. In *Figure 5* only samples with continuous stratified structures are dealt with as verified using SEM. As can be inferred from *Figure 5a* (PS-PPE/PE 100-0/ $X$ ), the strain-to-break shows an initial upswing at  $\sim 1 \mu\text{m}$  and increases with a decreasing PS-PPE layer thickness. The maximum strain-to-break is 100% and is observed for the 100-0/75 tape at a thickness of 0.4  $\mu\text{m}$ . Tapes containing  $< 75 \text{ wt}\%$  PE have a strain-to-break of  $< 10\%$  (more elements in the mixer resulted in discontinuous layers).

Adding 20 wt% PPE to the PS phase (PS-PPE/PE 80-20/ $X$ ; *Figure 5b*) gives roughly the same results (upswing at  $\sim 1 \mu\text{m}$ ) with the exception that the maximum strain-to-break of the tape is  $\sim 130\%$  for the 80-20/75 tape with a PS-PPE layer thickness of 0.5  $\mu\text{m}$ . (For the 80-20/ $X$  tapes the experimentally achievable minimum continuous PS-PPE layer thickness without the occurrence of rupture equals this.)

Only increasing the PPE content of the PS-PPE phase above 40 wt% allows for a substantial increase of the maximum number of mixing elements applicable in the static mixer before layer rupture occurs during processing. Consequently, the minimum attainable continuous PS-PPE layer thickness is significantly decreased to  $\sim 0.05 \mu\text{m}$ . *Figure 5c* shows the strain-to-break of the 60-40/ $X$  tapes versus the PS-PPE layer thickness. The 60-40/75 tape demonstrates initially the same behaviour as already described for 100-0/ $X$  and 80-20/ $X$  tapes: an initial upswing at  $\sim 1 \mu\text{m}$ . However, now also a maximum strain-to-break ( $\approx 125\%$ ) is observed for a layer thickness

of  $\sim 0.4 \mu\text{m}$ . Below this value the strain-to-break decreases to 70% at a layer thickness of 0.04  $\mu\text{m}$  (i.e. the minimum achievable experimental PS-PPE layer thickness). The strain-to-break of the 60-40/50 and 60-40/25 tapes now can be measured up to very thin layers and shows a significant increase if the PS-PPE layer thickness is below 0.1  $\mu\text{m}$ . From the optical micrographs taken during deformation (*Plate 1*) and the discussion here, it can be stated that there is a distinct difference in the two transitions found for this PS-PPE composition. The apparent brittle-to-ductile transition at the layer thickness of  $\sim 1 \mu\text{m}$ , as found for the 60-40/75 tape (and the 100-0/75 and 80-20/75 tapes as well), is correlated with the stress transfer mechanism, while the second transition (at  $\approx 0.1 \mu\text{m}$  for the 60-40/ $X$  tapes only) coincides with a change in deformation mechanism. Moreover, both the value of the critical thickness and the strain-to-break below the second transition agree very well with the data extracted from the core-shell rubber-modified PS-PPE 60-40 blends<sup>2</sup>.

Finally, for the PS-PPE/PE 40-60/ $X$  tapes only a single transition is found for all PS-PPE/PE compositions (*Figure 5d*) at a PS-PPE thickness of  $\sim 0.3 \mu\text{m}$ : a (critical) thickness that again correlates well with the critical matrix ligament thickness as already reported for the 40-60 blend determined with stress-strain measurements of core-shell rubber-modified 40-60 blends<sup>2</sup>. Also the maximum level of strain-to-break in the ductile region, i.e. below the critical layer/ligament thickness, agrees perfectly with the maximum macroscopic strain-to-break of core-shell rubber-modified 40-60 blends (70%)<sup>2</sup>.

#### Microscopy during tensile testing

In order to investigate the various transitions observed in *Figure 5*, uniaxial tensile testing is performed on the 60-40/75 tape at several PS-PPE layer thicknesses on a tensile stage mounted under an optical microscope (Minimat). *Plates 1a-c* show polarized optical transmission micrographs of a 60-40/75 tape having a PS-PPE layer thickness of 1.5  $\mu\text{m}$  taken at distinct strain levels (direction of load is horizontal). At 4% strain thin lines are visible perpendicular to the direction of load. The black thin lines probably correspond to small cracks preceded by

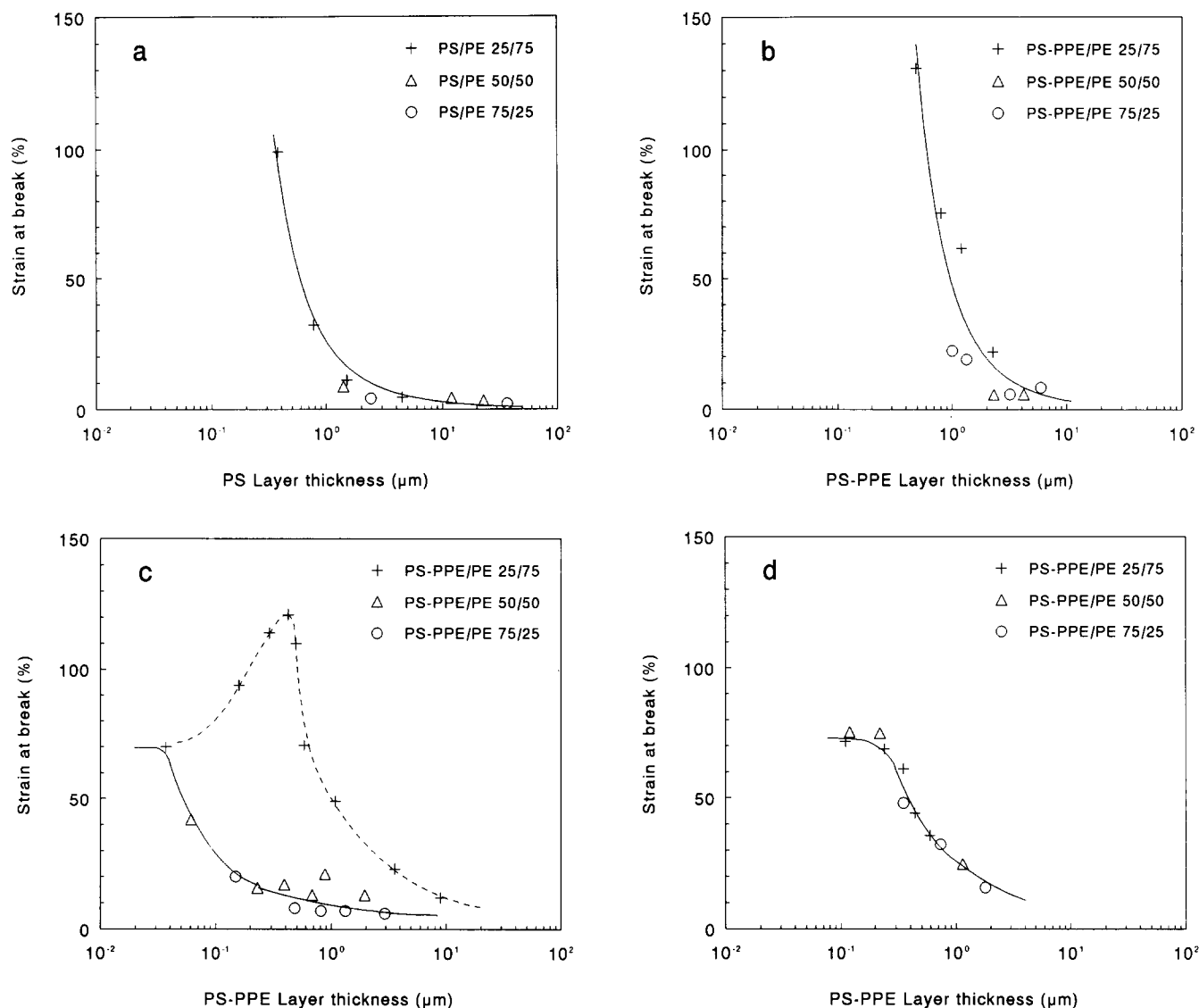


**Figure 5** Strain-at-break of several PS-PPE/PE tapes versus PS-PPE layer thickness: (a) 100-0/X; (b) 80-20/X; (c) 60-40/X; and (d) 40-60/X

crazes. Increasing the strain results in a strong increase in the number of cracks perpendicular to the load direction (*Plate 1c*, 8% strain). Decreasing the PS-PPE layer thickness to 0.5 μm (*Plates 1d-f*, corresponding to the tape possessing a maximum strain-to-break break of ~125%) results at the same strain level (e.g. 8%) in: (i) an increase of the number of cracks visible; and (ii) a more pronounced visibility of the cracks. A further decrease of the PS-PPE layer thickness (0.04 μm, *Plates 1g-i*, below the critical thickness demonstrated in ref. 2) drastically changes the optical observations: at any stage during the deformation no cracks can be detected. Moreover, the bright colours that are visible during the deformation under the optical microscope indicate massive plastic (shear) deformation. These microscopic observations demonstrate that a transition occurs from a crack-like deformation (preceded by crazes) at ~1 μm to a shearing type of deformation mechanism if the PS-PPE layer thickness is decreased below 0.05 μm.

*Figure 6* shows the stress-strain curves of two 60-40/75 tapes possessing a PS-PPE layer thickness of 0.29 μm (curve A) and 0.04 μm (curve B) respectively. Comparing both stress-strain curves confirms the two different deformation mechanisms occurring in both tapes as

determined with the optical microscope observations of *Plate 1*: curve A corresponds to the typical curve of a craze deforming polymer<sup>20</sup> (a constant stress level after the yield point; e.g. rubber-toughened PS<sup>21</sup>), while curve B shows the characteristics of a true shear deforming polymer ('strain hardening')<sup>20</sup>.

#### Modelling of the first transition

For PS-PPE layer thicknesses comparable with or larger than 0.5 μm cracks are already visible at low strains for the PS-PPE/PE 60-40/75 tape (*Plates 1c* and *f*) without causing a fatal macroscopic failure of the tape (*Figure 5c*). Similar observations are made in the area of fibre reinforced composites, where a rather stiff (low strain-to-break) fibre is embedded in a ductile polymeric matrix possessing a strain-to-break considerably higher than the fibre<sup>22,23</sup>. The observation that a fibre embedded in a polymeric matrix can be fractured several times along the fibre before final failure of the composite occurs is explained by the stress transfer mechanism<sup>22,23</sup>. This mechanism becomes operative if there is a substantial level of adhesion present between the fibre and the polymeric matrix, expressed by the matrix shear strength

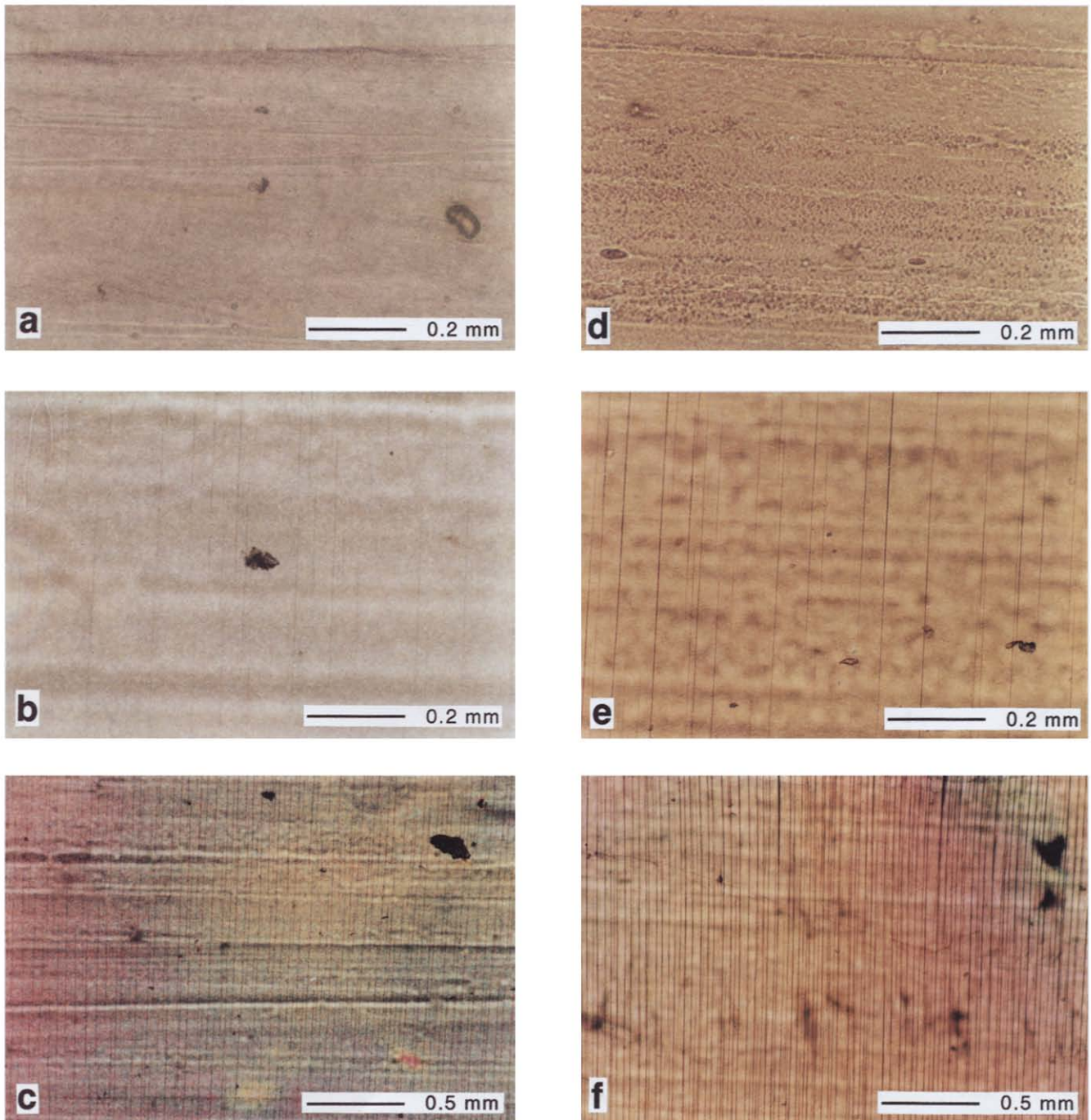


**Plate 1** Polarized optical micrographs of strained PS-PPE/PE 60-40/75 tapes for several PS-PPE layer thicknesses and strain levels: (a) 1.5  $\mu\text{m}$ , 0% strain; (b) 1.5  $\mu\text{m}$ , 4% strain; (c) 1.5  $\mu\text{m}$ , 8% strain; (d) 0.5  $\mu\text{m}$ , 0% strain; (e) 0.5  $\mu\text{m}$ , 4% strain; (f) 0.5  $\mu\text{m}$ , 8% strain; (g) 0.04  $\mu\text{m}$ , 0% strain; (h) 0.04  $\mu\text{m}$ , 4% strain; and (i) 0.04  $\mu\text{m}$ , 13% strain

or interfacial shear strength ( $\tau_m$ ) whichever is smaller. After breakage of the fibre stress can be built up by stress transfer from the matrix. The process of breakage continues until the transferred stress becomes lower than the strength of the fibre ( $F_{\text{max}}$ ). A simple force balance results in a correlation between  $\tau_m$  and  $F_{\text{max}}$  on the one hand and the critical transfer length ( $l_c$ ) and the fibre diameter ( $d_f$ ) on the other hand:

$$\frac{l_c}{d_f} = \frac{F_{\text{max}}}{2\tau_m} \quad (2)$$

Im *et al.*<sup>14</sup> carried out a similar analysis for microlayered composites which resulted in a relationship between  $\tau_m$ ,

$F_{\text{max}}$ ,  $l_c$  and  $t$ :

$$\frac{l_c}{t} = \frac{F_{\text{max}}}{2\tau_m} \quad (3)$$

where  $t$  is the layer thickness of the brittle component (i.e. the component possessing the lowest strain-to-break). Equation (3) implies that a decrease of the PS-PPE layer thickness (i.e. the 'brittle' component) by a factor of two upon the addition of one extra mixing element in the static mixer results in a decrease of  $l_c$  by the same factor of two and, consequently, in an increase of the macroscopic strain-to-break if it is assumed that the macroscopic strain-to-break of the multilayered tape is

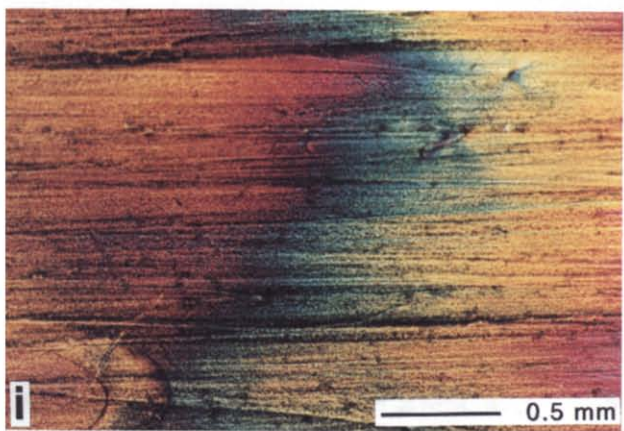
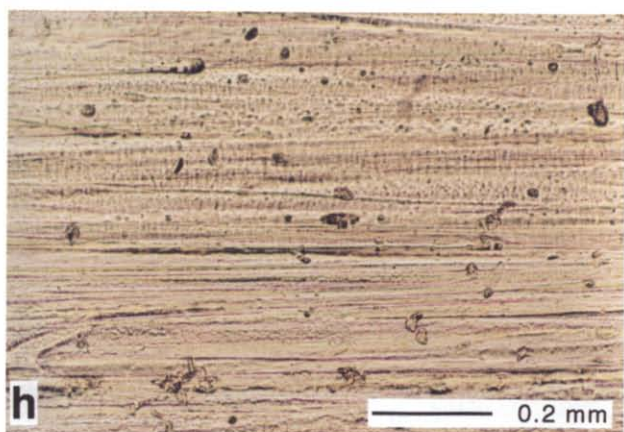
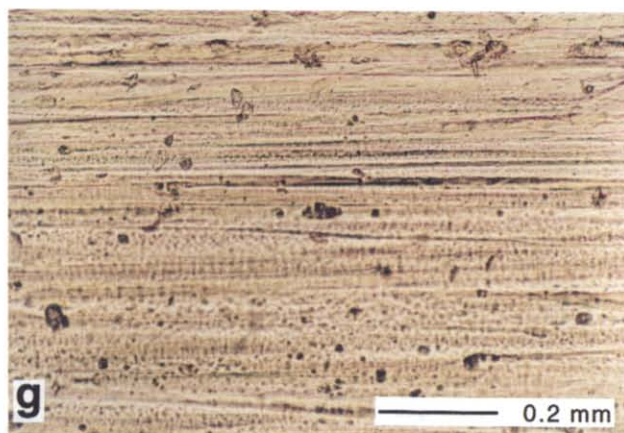


Plate 1 continued

directly correlated with the number of breakages along the length of the tape. Inspection of the transitions at  $\sim 1 \mu\text{m}$  observed for both the 100-0/75, 80-20/75 and 60-40/75 tapes (Figures 5a, b and c) experimentally verifies equation (3): for PS-PPE layer thicknesses below  $10 \mu\text{m}$  an increasing strain-to-break is observed with a decreasing PS-PPE layer thickness. The addition of an extra mixing element results in a reduction of the PS-PPE layer thickness by half and, consequently, in an increase of the strain-to-break of the tape roughly by a factor of two. For PS-PPE layer thicknesses below  $0.5 \mu\text{m}$  (only experimentally achievable for the 60-40/75 tape) the strain-to-break of the multilayered tape decreases with a decreasing layer thickness. This can be explained by the fact that the deformation mechanism of the PS-PPE layers starts to change from a craze-like deformation into

a shearing type of deformation (cf. Plates 1f and i). The crack-like deformation does not occur for layer thicknesses below  $0.05 \mu\text{m}$ . Instead the PS-PPE/PE tape fails after complete homogeneous shear deformation of the PS-PPE phase up to the theoretical strain-to-break ( $70\%$  for the 60-40 blend<sup>2</sup>).

For PS-PPE/50 and PS-PPE/25 tapes the stress transfer mechanism as described above seems to be absent (Figure 5). This can be ascribed to the fact that upon decreasing the PE content of the tape, fracture of a PS-PPE layer will result in a higher stress level in the neighbouring PE layers. Hence, a fracture of the PE layers is likely to occur immediately after the first fracture of a PS-PPE layer resulting in a fatal failure of the whole tape.

Inspection of Figure 5d only reveals a single brittle-to-ductile transition at  $\sim 0.25 \mu\text{m}$ , obviously the stress transfer mechanism is not operative in these tapes or coincides with the brittle-to-ductile transition induced by the change in deformation mechanism<sup>2</sup>.

#### Increase in interlayer adhesion

Exploiting the stress transfer mechanism (by increasing the interlayer adhesion between PS-PPE and PE) should, finally, result in a PS-PPE/PE tape possessing the strain-to-break of pure PE. This hypothesis is verified by the introduction of a third component in the multilayered PS-PPE/PE tapes: a diblock copolymer based on styrene and hydrogenated isoprene rubber. In Figure 7 a SEM micrograph is shown of a PS/PE/BC 25/74/1 (w/w/w) tape having a PS layer thickness of  $\sim 1 \mu\text{m}$ . The diblock copolymer is not detectable on the SEM micrograph (only 1 wt% is present) but it is most likely positioned at the interface with the styrene part of the diblock copolymer positioned in the PS layers and the hydrogenated isoprene rubber block in the PE layers. The presence of the diblock copolymer should increase the interlayer adhesion (and therefore also the interfacial shear strength,  $\tau_m$ ) significantly<sup>24,25</sup>. Examination of equation (3) reveals that an increase in  $\tau_m$  results in a decrease of  $l_c$  at a constant layer thickness. Stress-strain analysis of the tape shown in Figure 7 results in a strain-to-break of 230% (i.e. the strain-to-break of

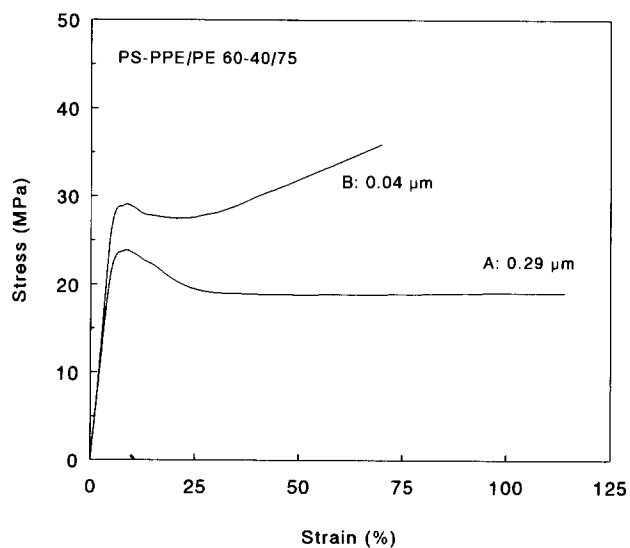
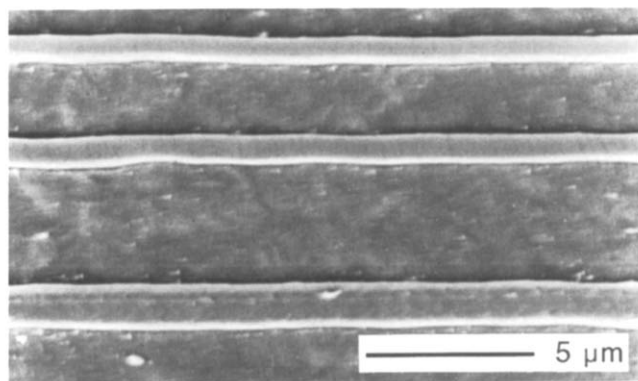


Figure 6 Stress-strain curves of PS-PPE/PE 60-40/75 tapes for two different PS-PPE layer thicknesses



**Figure 7** SEM micrograph of a multilayered PS/PE/BC 25/74/1 (w/w/w) tape possessing a PS layer thickness of 1  $\mu\text{m}$

pure PE) which is considerably higher than the strain-to-break of the corresponding PS/PE 25/75 tape (no diblock copolymer present) having the same PS layer thickness (30%, cf. *Figure 5a*).

#### Modelling of the second transition

In conclusion, generally two transitions are found in the multilayered tapes. The first transition only occurs at a PS-PPE layer thickness of  $\sim 1 \mu\text{m}$  if relatively thick PE spacing layers are present. This transition is due to the stress transfer between the (slightly) adhering layers. The second transition is found if the layers can be made thin enough (which is dependent on the viscosity ratio) and coincides with a change in deformation mechanism from crazing to shearing. Thus, after a careful and critical evaluation of the results obtained with the stratified structures it can be stated that the concept of a critical thickness, below which brittle polymers become ductile, is not only valid for thin matrix ligaments<sup>1,2</sup> but is also applicable to thin films (*Figure 5c*, transition at 0.05  $\mu\text{m}$ ; *Figure 5d*, transition at 0.25  $\mu\text{m}$ ). The maximum strain-to-break in the ductile region could be explained by the theoretical maximum elongation of the polymer network ( $\lambda_{\text{max}}$ ) and the absolute value of the critical thickness could be quantitatively understood from a simple energy-based model (see parts 2 and 4<sup>2,7</sup>). This model is, however, only applicable to the thin film experiments if additional assumptions with respect to the matrix volume supplying the stored elastic energy are made. It is therefore interesting to reproduce an alternative explanation for the thickness transition in thin films that focuses on the change in deformation mechanism and is derived from the established theory of Kramer for craze growth<sup>8,26</sup>. If it is postulated that a craze structure should contain at least two craze fibrils, this minimum thickness ( $L_{\text{min}}$ ), in which the craze structure just can fit, can be calculated from the fastest growing fibril spacing  $D_{\text{o},\text{tr}}^*$  (see Appendix):

$$L_{\text{min}} = \frac{16\Gamma}{\sigma_y(1 - \lambda_{\text{max}}^{-1/2})} + 2h \quad (4)$$

where  $\Gamma$  is the surface energy involving the breakage of chains,  $\sigma_y$  is the yield stress,  $\lambda_{\text{max}}$  is the theoretical maximum extension ratio of the entanglement network and  $h$  is the thickness of the active zone layer at the craze/bulk interface. Taking for PS:  $\Gamma = 0.08 \text{ J m}^{-2}$  (ref. 8),  $\sigma_y = 82.8 \text{ MPa}$  (ref. 27),  $\lambda_{\text{max}} = 4.2$  (ref. 26) and  $h = 25 \text{ nm}$  (ref. 28) results in a value of  $L_{\text{min}}$  of 80 nm, a value that is rather close to the value derived from the energy-based model that resulted in 55 nm.

As Kramer suggested<sup>29</sup>, a better approximation can be made if not the fastest growing fibril spacing is considered but the fibril spacing less than the fastest growing one, that widens at a reduced rate. The transition from crazing to shearing occurs if the craze widening velocity is equal to the velocity of widening a shear deformation zone. Combining the estimated fibril spacing ( $D_{\text{o},\text{tr}}$ ) at which the transition occurs from crazing to shear deformation with the assumption that this minimum thickness contains just two craze fibrils results in a somewhat different expression for  $L_{\text{min},\text{tr}}$ :

$$L_{\text{min},\text{tr}} = 4h - h \sqrt{4 - \frac{32\Gamma}{\sigma_y h (1 - \lambda_{\text{max}}^{-1/2})}} \quad (5)$$

(see Appendix for the derivation). Using the same data for PS as used above, results in a value of  $L_{\text{min},\text{tr}} = 69 \text{ nm}$ , a value that is even closer to the one calculated with the energy-based model. The critical thickness for the other PS-PPE blends analysed in this study according to equations (4) ( $L_{\text{min}}$ ) and (5) ( $L_{\text{min},\text{tr}}$ ) is shown in *Figure 8* (broken curves; the value of  $h$  is assumed to be independent of the PS-PPE composition, which might be incorrect). For comparison, the critical thickness according to the energy-based model of part 2 is also incorporated in this figure (full curve)<sup>2</sup>. Experimentally, the critical thickness associated with a change in deformation mechanism could only be determined for the 60-40/X and 40-60/X tapes. The critical matrix ligament thickness determined via core-shell rubber-modification of the PS-PPE 100-0, 80-20, 60-40 and 40-60 blends is also shown in *Figure 8*. Inspection of *Figure 8* reveals that all three models result in a satisfying prediction of the critical thickness for the several PS-PPE blends. However, the validity of the model predictions of the critical thickness via equations (4) and (5) is only limited to polymeric systems where the critical thickness is clearly associated with a change in deformation mechanism. For the epoxide systems discussed in part 3 of this series<sup>6</sup>, only the energy-based model for the critical thickness can be used.

Apparently, the low value of the interlayer adhesion is already sufficiently high to make the stress transfer

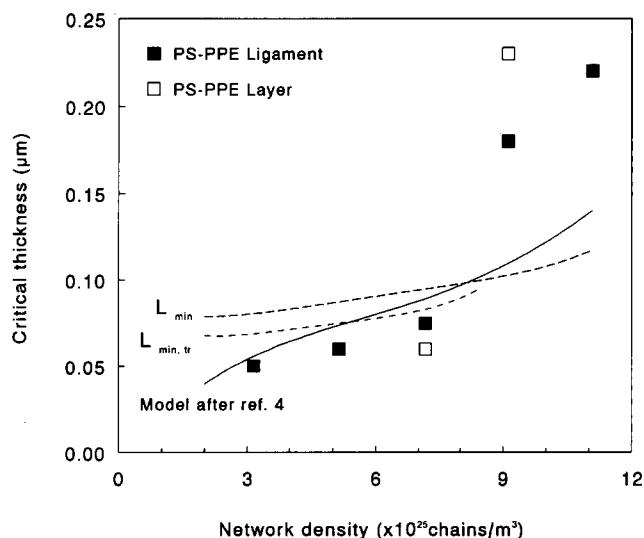


**Figure 8** Critical thickness versus the matrix entanglement density ( $\nu_e$ ) for the various PS-PPE blends. The curves are according to the various models. For details, see text



mechanism noticeable on a macroscopic scale. However, for the change in deformation mechanism upon decreasing the PS-PPE layer thickness the low level of interlayer adhesion seems to have no profound influence since the critical matrix ligament thickness reported for the non-adhering core-shell rubber-modified 60-40 and 40-60 blends<sup>2</sup> coincides with the critical PS-PPE layer thickness observed in this study.

## CONCLUSIONS

The strain-to-break of PS-PPE/PE 100-0/75, 80-20/75 and 60-40/75 tapes can be increased significantly by a decrease of the PS-PPE layer thickness ( $d$ ) to  $d \approx 1 \mu\text{m}$ . The origin of the increased strain-to-break of these tapes is explained by a stress transfer mechanism as revealed by optical light microscopy during tensile testing, i.e. PE locally inhibits crack growth after the PS-PPE layer breakage and allows for a multiple fracture of each single PS-PPE layer as a result of the (low) level of interlayer adhesion between PS-PPE and PE ( $G_{ic} \approx 5 \text{ J m}^{-2}$ ). A further decrease of  $d$  results (only for the 60-40/75 tape, where the layer thickness can be decreased further without layer rupture) in a maximum strain-to-break at a layer thickness of  $0.4 \mu\text{m}$ , followed by a decrease of the strain-to-break, finally, to a value of 70% at a layer thickness of  $0.04 \mu\text{m}$ . The latter transition coincides with a change in deformation mechanism (optical light microscopy) and corresponds to the critical thickness as already reported in part 2 of this series<sup>2</sup> for the non-adhering core-shell rubber-modified PS-PPE 60-40 blend.

For the PS-PPE/PE 60-40/50, 60-40/25 and 40-60/ $X$  tapes only one transition, induced by a change in layer thickness, could be detected that is correlated with a change in deformation mechanism. Again, this transition coincides with a change in deformation mechanism from multiple cracking (preceded by crazing) to shear deformation as demonstrated for rubber-modified PS-PPE blends where the (local) thickness is controlled by the ligament thickness between the non-adhering rubbery particles. The critical thickness for transitions associated with a change in deformation mechanism is not only predicted satisfactorily by the previously introduced energy-based model<sup>2</sup> but can also be understood from the well established theory of Kramer for craze growth<sup>8,26</sup>.

The introduction of a diblock copolymer between the PS and PE layers enables a practical exploitation of the stress transfer mechanism: the stress transfer mechanism already becomes maximum operative at PS-PPE layer thicknesses of  $\sim 1 \mu\text{m}$ . This results in a (quasi) macroscopic strain-to-break of a PS/PE/BC 74/25/1 tape of 230%, i.e. the strain-to-break of pure PE, where the individual PS layers are fragmented many times along the length of the tape without initiating a fatal macroscopic failure.

## ACKNOWLEDGEMENTS

The authors kindly wish to thank A. Hiltner and E. Baer (Center for Applied Polymer Research, Case Western Reserve University, Cleveland) for their stimulating discussions and for providing the necessary facilities to perform the tensile experiments under the optical microscope. E. J. Kramer (Department of Materials

Science and Engineering, Cornell University, Ithaca) is gratefully acknowledged for his critical comments and alternative model for the tapes. This work is supported by the Foundation for Polymer Blends (SPB).

## REFERENCES

- 1 Van der Sanden, M. C. M., Meijer, H. E. H. and Lemstra, P. J. *Polymer* 1993, **34**, 2148
- 2 Van der Sanden, M. C. M., Meijer, H. E. H. and Tervoort, T. A. *Polymer* 1993, **34**, 2961
- 3 Wilson, G. M. and Khomami, B. J. *Non-Newt. Fluid Mech.* 1992, **45**, 355
- 4 Wilson, G. M. and Khomami, B. J. *Rheol.* 1993, **37**, 315
- 5 Wilson, G. M. and Khomami, B. J. *Rheol.* 1993, **37**, 341
- 6 Van der Sanden, M. C. M. and Meijer, H. E. H. *Polymer* 1993, **34**, 5063
- 7 Van der Sanden, M. C. M. and Meijer, H. E. H. *Polymer* 1994, **35**, 2774
- 8 Kramer, E. J. and Berger, L. L. *Adv. Polym. Sci.* 1990, **91/92**, 1
- 9 Radford, J. A., Alfrey Jr, T. and Schrenk, W. J. *Polym. Eng. Sci.* 1973, **13**, 216
- 10 *US Pat. 3 711 176*, 1973
- 11 Schrenk, W. J. and Alfrey Jr, T. *Polym. Eng. Sci.* 1969, **9**, 393
- 12 Ma, M., Im, J., Hiltner, A. and Baer, E. J. *Appl. Polym. Sci.* 1990, **40**, 669
- 13 Ma, M., Vijayan, K., Hiltner, A. and Baer, E. J. *Mater. Sci.* 1990, **25**, 2039
- 14 Im, J., Baer, E. and Hiltner, A. in 'High Performance Polymers' (Eds E. Baer and A. Moet), Hanser Publishers, Munich, 1991, pp. 175-198
- 15 Bazhenov, S. L., Sellitti, C., Hiltner, A. and Baer, E. J. *Appl. Polym. Sci.* in press
- 16 Meijer, H. E. H. and Janssen, J. M. H. in 'Mixing and Compounding—Theory and Practice' (Eds I. Manas-Zloczower and Z. Tadmor), Progress in Polymer Processing Series, Carl Hanser Verlag, Munich, in press
- 17 Nielsen, L. E. and Buchdahl, R. J. *Appl. Phys.* 1950, **21**, 488
- 18 Beardmore, P. and Rabinowitz, S. J. *Mater. Sci.* 1975, **10**, 1763
- 19 Bazhenov, S. L., Sellitti, C., Hiltner, A. and Baer, E. J. *Appl. Polym. Sci.* in press
- 20 Kinloch, A. J. and Young, R. J. 'Fracture Behaviour of Polymers', Elsevier Applied Science, London, 1985
- 21 Bucknall, C. B. 'Toughened Plastics', Applied Science, London, 1977
- 22 Rosen, B. W. *J. AIAA* 1964, **2**, 1985
- 23 Broutman, L. J. and Krock, R. H. 'Modern Composite Materials', Addison-Wesley, Reading, MA, 1967, Ch. 1
- 24 Brown, H. R., Deline, V. R. and Green, P. F. *Nature* 1989, **341**, 221
- 25 Brown, H. R. *Macromolecules* 1989, **22**, 2859
- 26 Kramer, E. J. *Adv. Polym. Sci.* 1983, **52/53**, 1
- 27 Kambour, R. P. *Polym. Commun.* 1983, **24**, 292
- 28 Miller, P. and Kramer, E. J. *J. Mater. Sci.* 1991, **26**, 1459
- 29 Kramer, E. J. personal communication, 1993

## APPENDIX

*The derivation of the critical thickness in films from craze growth analysis according to Kramer<sup>29</sup>*

The following expression for the fastest growing fibril spacing ( $D_o^*$ ), that dominates at any tensile stress,  $S$ , and maximizes the pressure gradient ( $\Delta\sigma$ ), can be derived from an updated version of the original model of Kramer<sup>8,26</sup>:

$$D_o^* = \frac{8\Gamma}{\beta S(1 - \lambda_{\max}^{-1/2})} \quad (\text{A1})$$

where  $\Gamma$  is the surface energy of the polymeric material,  $\beta$  is a constant of the order one [see equation (11) of ref. 8],  $S$  is the average tensile stress on the craze interface and  $\lambda_{\max}$  is the natural draw ratio of the polymer [cf. equation (13) of ref. 8 where it was assumed that  $r \approx D_o/2$  and the factor  $1/(1 - \lambda_{\max}^{-1/2})$  was ignored].

If we assume that it takes about one active zone thickness ( $h$ ) to build up the hydrostatic tension necessary

to stabilize the small radius of curvature on the outsides of the fibrils and that the minimum thickness ( $L_{\min}$ ) into which the fibril structure fits contains two fibrils,  $L_{\min}$  can be expressed in  $D_0$  and  $h$ :

$$L_{\min} = 2(D_0 + h) \quad (\text{A2})$$

Combination of equations (A1) and (A2) finally results in:

$$L_{\min} = \frac{16\Gamma}{\beta S(1 - \lambda_{\max}^{-1/2})} + 2h \quad (\text{A3})$$

which can be rewritten to equation (4) if we take  $\beta$  to be 1 and assume the tensile stress  $S$  to be equal to the lower yield stress ( $\sigma_y$ ) of the polymer.

A better estimation of  $L_{\min}$  can be made if at the thickness transition not the craze fibril spacing is considered that grows the fastest, but the craze fibril spacing  $D_{0,\text{tr}}$  that grows at a reduced rate ( $v$ ), equal to the widening velocity of a shear deformation zone ( $v_{\text{DZ}}$ ). For the craze widening velocity,  $v$ , we can write that it scales as [see equation (9) of ref. 8]:

$$v \sim \left( \frac{h\Delta\sigma}{\sigma_{fc}} \right)^n \quad (\text{A4})$$

where  $\sigma_{fc}$  is a flow stress of the material in the active zone at a certain reference strain rate and  $n$  is an exponent ( $\gg 1$ ) which describes the stress dependence in the active zone. The widening velocity of a shear deformation zone is assumed to possess the same power law:

$$v_{\text{DZ}} \sim (S/\sigma_y)^n \quad (\text{A5})$$

where  $S$  is the average stress on the bulk/deformation zone interface and  $\sigma_y$  is the yield stress at the same

reference strain rate as above. Assuming that the two exponents  $n$  are equal the transition occurs if  $v = v_{\text{DZ}}$ :

$$\Delta\sigma = \frac{\sigma_{fc} S}{\sigma_y h} \quad (\text{A6})$$

At the transition we assume that  $S \approx \sigma_y$ , which with equations (A2) and (10), (11) and (12), where  $r \approx D_0/2$  is replaced by  $r \approx D_0/[2(1 - \lambda_{\max}^{-1/2})]$  analogous to the additional factor introduced in equation (A1), of ref. 8, leads to the following quadratic equation:

$$\left( \frac{L_{\min}}{2h} - 1 \right)^2 - B \left( \frac{L_{\min}}{2h} - 1 \right) + C = 0 \quad (\text{A7})$$

where  $B$  and  $C$  are the following dimensionless parameters:

$$B = \frac{2\beta\sigma_y}{\sigma_{fc}} \quad (\text{A8})$$

and

$$C = \frac{8\Gamma}{\sigma_{fc} h (1 - \lambda_{\max}^{-1/2})} \quad (\text{A9})$$

The smallest solution of equation (A7) corresponds to the material thickness ( $L_{\min,\text{tr}}$ ) smaller than the one that contains two craze fibrils and grows the fastest [equation (A3)]. If it is assumed that  $\sigma_{fc} \approx \sigma_y$  this solution can be written as:

$$L_{\min,\text{tr}} = 4h - h \sqrt{4 - \frac{32\Gamma}{\sigma_y h (1 - \lambda_{\max}^{-1/2})}} \quad (\text{A10})$$

which is equation (5).